

Silicon-based all-optical photonic crystal neuromorphic synapses using $\text{Ge}_2\text{Sb}_2\text{Te}_5$: supplement

AMIR HOSSEIN ABDOLLAHI NOHOJI, PARVIZ KESHAVARZI, AND
MOHAMMAD DANAIE* 

Faculty of Electrical and Computer Engineering, Semnan University, Semnan, Iran

**danaie@semnan.ac.ir*

This supplement published with Optica Publishing Group on 16 July 2025 by The Authors under the terms of the [Creative Commons Attribution 4.0 License](#) in the format provided by the authors and unedited. Further distribution of this work must maintain attribution to the author(s) and the published article's title, journal citation, and DOI.

Supplement DOI: <https://doi.org/10.6084/m9.figshare.29457944>

Parent Article DOI: <https://doi.org/10.1364/OPTCON.560333>

SUPPLEMENTAL

SILICON-BASED ALL-OPTICAL PHOTONIC CRYSTAL NEUROMORPHIC SYNAPSES USING $\text{Ge}_2\text{Sb}_2\text{Te}_5$: SUPPLEMENTAL DOCUMENT

Sensitivity of the proposed structure to the radii of holes A2 and A5.

In Fig. S1(a), changes in the radii of A2 and A5 have the greatest effect on the resonance wavelength when the input is sent from ports 1 to 2. In contrast, changes in B2 and B5 radii have no significant effect on resonant wavelength transmission. In Fig. S1(b), changes in the radius of holes B2 and B5 have the most significant effect on the transition from ports 3 to 4, while holes A2 and A5 show the slightest impact. The rod radius as a function of wavelength is been determined and depicted in each figure, utilizing MATLAB's Curve Fitting Toolbox for precise modeling.

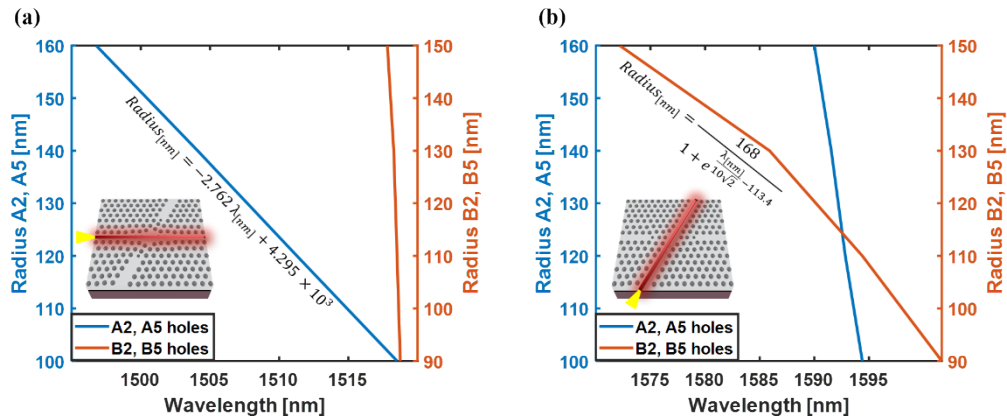


Fig. S1. Maximum transmission wavelength based on variation in radii of holes A2, A5, and B2, B5 for input from (a) ports 1 to 2, and (b) ports 3 to 4. The radii of holes A2 and A5 and holes B2 and B5 have the greatest effect on the transmission wavelength in their respective waveguides.

$\text{Ge}_2\text{Sb}_2\text{Te}_5$ Phase Change Material.

Fig. S2 shows the real and imaginary parts of the refractive index for GST and GSST materials at different wavelengths [20,35].

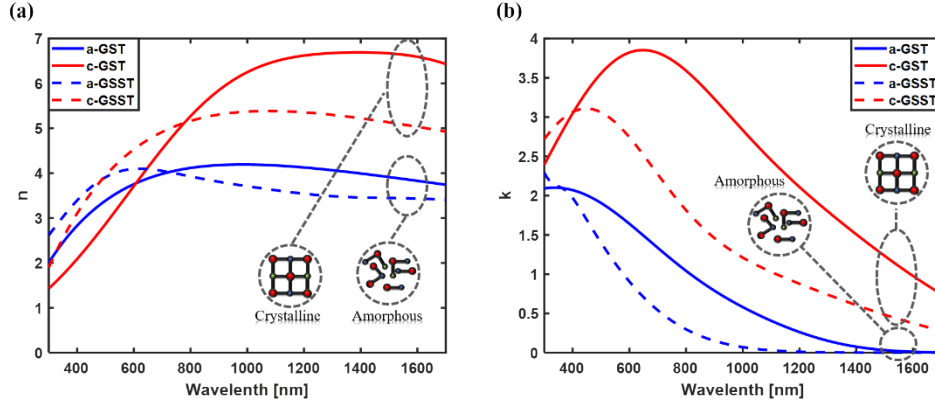


Fig. S2. (a) Real part, and (b) Imaginary part of GST and GSST refractive index. In the wavelength range of 1500-1600 nm (indicated by the gray box), a significant difference is observed in the real and imaginary parts of the refractive index for the GST and GSST materials.

Fig. S3 illustrates the phase diagram and transition process between the crystalline and amorphous states in GST materials. Moving toward the GeTe material along the line section, the melting temperature (T_m), glass transition temperature (T_g), and activation energy increase, while the crystallization speed decreases. Materials such as Se_2Te_3 can be used to increase the crystallization speed, but these materials are not stable enough. However, by choosing the $\text{Ge}_2\text{Sb}_2\text{Te}_5$ material, a favorable crystallization speed with relatively good stability can be achieved.

To transform GST material from an amorphous state to a crystalline state, the temperature of GST must be higher than the T_g and lower than the T_m . These conditions can be provided by applying pulses of low amplitude and high duration to heat the GST. Also, for GST to become amorphous, the temperature of GST must be raised above its melting point to liquefy and then rapidly cool. For this purpose, GST can be converted from the crystalline state to the amorphous state by applying a high-amplitude and short-duration pulse [77].

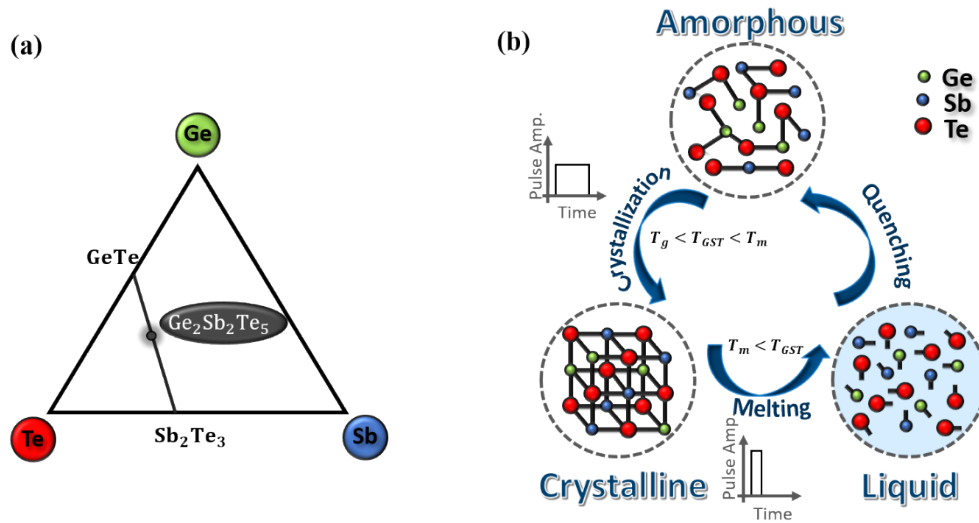


Fig. S3. (a) GST-PCM phase diagram, and (b) the transition process of GST-PCM.

Optimization of the radius of PCM rods.

The transition from ports 1 to 2 under the conditions of amorphous and fully crystalline states for GST and GSST rods is shown in Fig. S4. Actually, Fig. S4(a), (b) shows that by choosing the optimal radius of the PCM rod, a significant effect on the resonance wavelength transmission can be obtained. This capability is very critical in the design and optimization of optical devices.

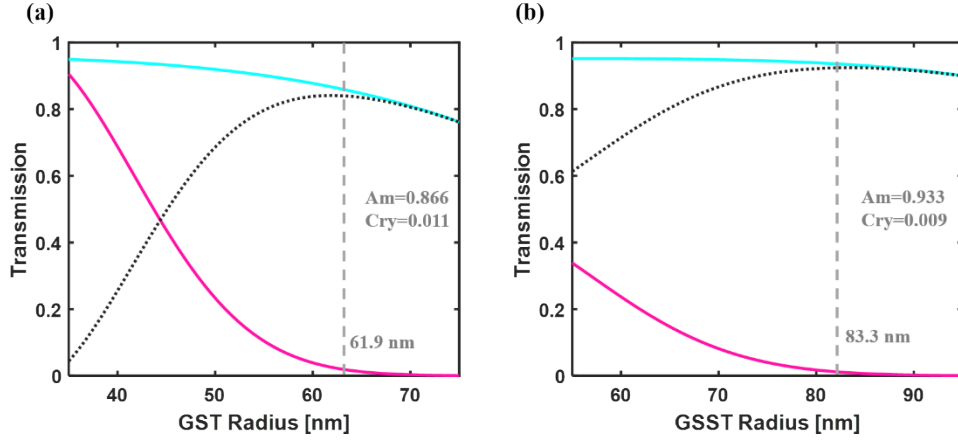


Fig. S4. Transmission from ports 1 to 2 for the proposed structure in both amorphous and crystalline states using (a) GST, and (b) GSST materials. For GST materials, the optimum radius of PCM rods to achieve the greatest discrimination between amorphous and crystalline states is 61.9 nm, while for GSST materials, it is 83.3 nm. (Cyan: Amorphous, magenta: Crystalline, and black dotted: Difference rate)

Fabrication tolerance and structural sensitivity analysis.

To assess the structural robustness and fabrication tolerance of the proposed photonic crystal architecture, an extensive sensitivity analysis has been conducted with respect to dimensional variations that may arise during the fabrication process. This supplementary section presents additional simulation results that extend the findings of the main manuscript by evaluating the impact of key geometric perturbations on the device's optical response.

Figure S5 illustrates the effect of ± 5 nm variations in the radii of selected holes (A3–A4, B3–B4, C3–C4, and C2–C5) on the transmission response for both input directions. The results indicate that the structure maintains acceptable optical performance under moderate deviations in hole dimensions.

Furthermore, Figure S6 illustrates the effect of GST rods' radii fluctuations on the resonance wavelength shift. The analysis reveals that the wavelength tuning remains within a controllable range, and the overall optical behavior of the structure is preserved across practical fabrication variations.

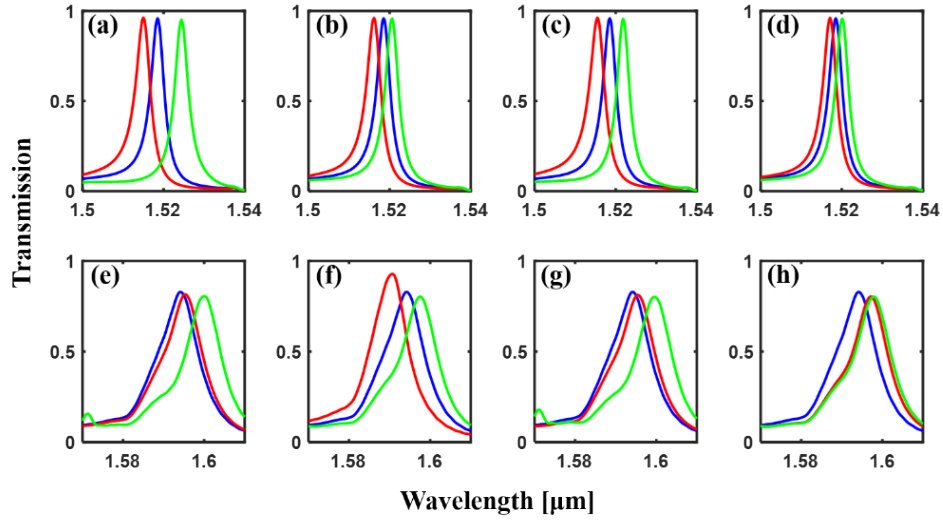


Fig. S5. Transmission spectra for variations in hole radii: (a–d) Transmission from ports 1 to 2, and (e–h) Transmission from ports 3 to 4, corresponding to ± 5 nm changes in the radii of holes (A3–A4, B3–B4, C3–C4, and C2–C5). Red lines represent a +5 nm increase, and green lines represent a –5 nm decrease in the respective hole radii.

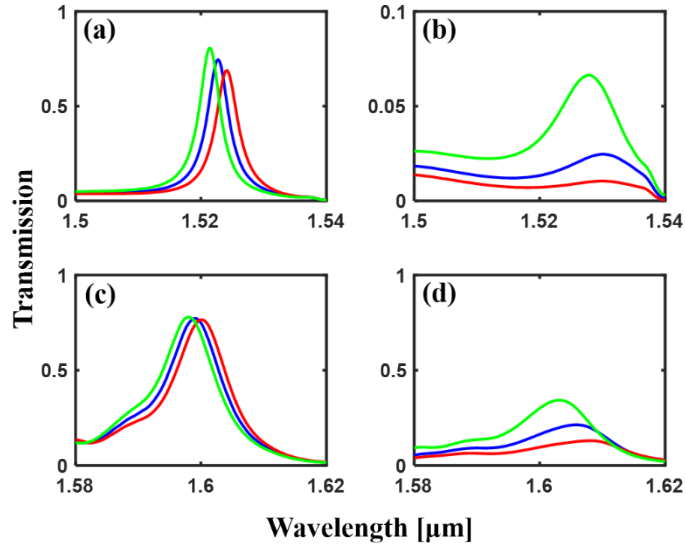


Fig. S6. Transmission spectra for ± 5 nm variations in GST rod radii: (a, b) from ports 1 to 2, and (c, d) from ports 3 to 4. Red: +5 nm, Green: –5 nm.

References

1. J. Feldmann, N. Youngblood, C. D. Wright, et al., "All-optical spiking neurosynaptic networks with self-learning capabilities," *Nature* **569**, 208–214 (2019).
2. M. Miscuglio, J. Meng, O. Yesiliurt, et al., "Artificial synapse with mnemonic functionality using GSST-

- based photonic integrated memory," in *2020 International Applied Computational Electromagnetics Society Symposium (ACES)* (2020), pp. 1–3.
3. S. Abdollahramezani, O. Hemmatyar, H. Taghinejad, et al., "Tunable nanophotonics enabled by chalcogenide phase-change materials," *Nanophotonics* **9**, 1189–1241 (2020).